Threshold-Voltage-Based Regional Modeling of MOSFETs with Symmetry and Continuity

Siau Ben Chiah*, Xing Zhou*, Karthik Chandrasekaran*,
Khee Yong Lim**, Lap Chan**, and Sanford Chu**

*School of Electrical & Electronic Engineering, Nanyang Technological University
Nanyang Avenue, Singapore 639798, exzhou@ntu.edu.sg
**Chartered Semiconductor Manufacturing Ltd, 60 Woodlands Industrial Park D, St. 2, Singapore 738406

ABSTRACT

This paper presents a unified threshold-voltage-based (V_t-based) MOSFET model, which maintains source–drain symmetry and allows accurate prediction of transconductance (g_m) and drain conductance (g_{ds}) and their derivatives (g_m' and g_{ds}') with smooth transitions across regions of operation. This has been achieved based on our previous unified source-extrapolated V_t-based model but re-derived with bulk reference for the drain current (I_{ds}). The unified model combines V_t-based model in strong inversion with surface-potential-based (Ψ_s-based) model in subthreshold with smooth transitions (in function as well as higher-order derivatives) across linear/saturation and weak/strong-inversion regions. It has been verified with the experimental data from a 0.18-μm CMOS shallow trench isolation (STI) technology wafer.

Keywords: Deep-submicron MOSFET, symmetry, threshold voltage, drain current, surface potential.

1 INTRODUCTION

Starting from the Meyer's model [1], V_t-based models have been the standard for decades in MOSFET compact models (CMs) for circuit simulation. However, in recent CM developments, more attention is focused on mixed-signal and low-power applications in which requirements for smooth transitions across different regions of operation become increasingly important. This becomes the challenge for V_t-based models to continue to survive as a standard for MOSFETs. Furthermore, a major problem associated with V_t-based models is symmetry, as seen in the BSIM model [2], which has been attributed to being source referenced. However, as pointed out in [3], source-reference and bulk-reference are essentially equivalent. A V_t-based model, in which V_t is the source-extrapolated threshold voltage, does not necessarily mean asymmetry as long as the drain-current equation is derived with bulk as the reference; likewise, a bulk-referenced model does not necessarily guarantee symmetry if velocity-saturation and lateral-field mobility are not handled properly.

In this paper, we focus on further development of the unified V_t-based model based on our previous source-referenced model, Xsim [4], but re-derive with bulk reference for the drain current (I_{ds}). In Section 2, formulation of the bulk-referenced I_{ds} and V_t models as well as parameter extraction is presented. Benchmark tests are carried out to verify the model continuity and symmetry, which are discussed in Section 3, together with experimental verification of the model.

2 MODEL FORMULATION AND PARAMETER EXTRACTION

The drain current equation based on charge-sheet approximation can be formulated as the drift current

$$I_{drift}(y) = \mu_{eff} W_{eff} Q_i(y)\, d\Psi_s(y)/dy \tag{1a}$$

and the diffusion current

$$I_{diff}(y) = \mu_{eff} W_{eff} v_{th}\, dQ_i(y)/dy \tag{1b}$$

where $\Psi_s(y)$ is the position-dependent surface potential,

$$Q_i(y) = C_{ox}\left[V_{gb} - V_{FB} - \Psi_s(y)\right] - Q_b(y) \tag{2a}$$

is the inversion charge along the channel, and

$$Q_b(y) = C_{ox}\gamma\sqrt{\Psi_s(y)} \tag{2b}$$

is the bulk charge. Rearranging (1a) and integrating across the channel from source ($y = 0$) to drain ($y = L_{eff}$), with the boundary conditions $\Psi_{s0} = 2\phi_F + V_{sb}$ and $\Psi_{sL} = 2\phi_F + V_{db}$:

$$\int_0^{L_{eff}} I_d(y)dy = \mu_{eff} W_{eff} \int_{\Psi_{s0}}^{\Psi_{sL}} Q_i d\Psi_s\,,$$

it can be shown [3] that the drift current is given by

$$I_{drift} = \beta_n\left[(V_{gs} - V_t)V_{ds} - \tfrac{1}{2} A_b V_{ds}^2\right], \tag{3}$$

in which

$$V_t = V_{FB} + \phi_{s0} + \gamma\sqrt{\phi_{s0}} - (A_b - 1)V_{bs} \tag{4}$$

$$A_b = 1 + \gamma \big/ \left(2\sqrt{\phi_{s0}}\right) \tag{5}$$

for the bulk-referenced model, which are different in form from the source-referenced model. In the above equations, V_{FB} is the flat-band voltage, $v_{th} = kT/q$ is the thermal voltage, $\phi_{s0} = 2\phi_F$ is the ("pinned") surface potential at strong inversion, $\gamma = (2q\varepsilon_{Si}N_{ch})^{1/2}/C_{ox}$ is the body factor, and $\beta_n = \mu_{eff}C_{ox}(W_{eff}/L_{eff})$ is the gain factor.

Similarly, for the diffusion current, by rearranging (1b) and integrating from source to drain, and taking the source and drain end inversion charge as

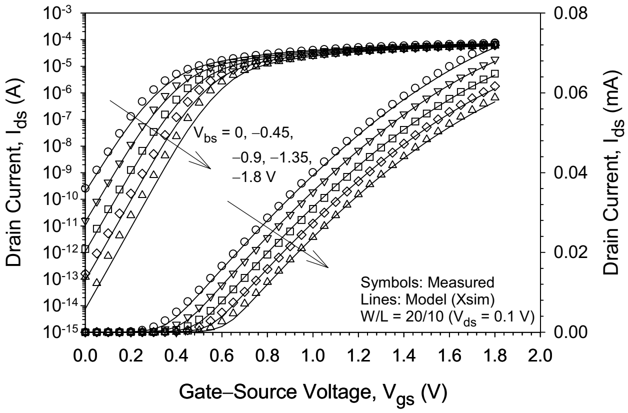

(a)

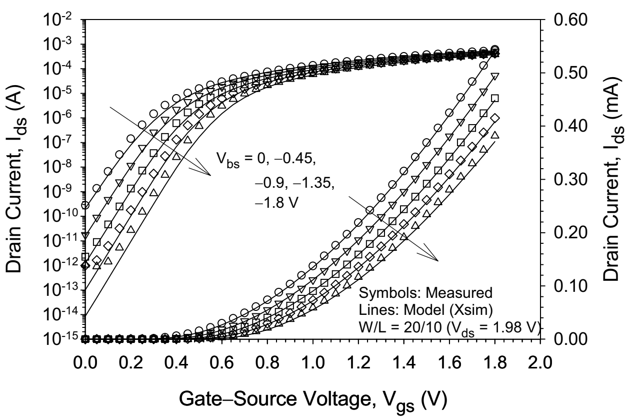

(b)

Figure 1: $I_{ds} - V_{gs}$ characteristics (V_{bs} = 0/–1.8 V at V_{ds} = 0.1 V fitted; others predicted) in (a) linear and (b) saturation regions for the L = 10-μm device.

$$Q_{i,s} \approx \frac{\gamma C_{ox}}{2\sqrt{\Psi_s}} v_{th} e^{(\Psi_s - 2\phi_F - V_{sb})/v_{th}} \tag{6a}$$

$$Q_{i,d} \approx \frac{\gamma C_{ox}}{2\sqrt{\Psi_s}} v_{th} e^{(\Psi_s - 2\phi_F - V_{db})/v_{th}} \tag{6b}$$

respectively, the compact diffusion current can be derived:

$$I_{diff} = \beta_n v_{th}^2 \left(C_d / C_{ox}\right) e^{(V_{gs} - V_t)/(n v_{th})} \left(1 - e^{-V_{ds}/v_{th}}\right) \tag{7}$$

where

$$C_d = \gamma C_{ox} \big/ 2\sqrt{\phi_{sub}} \tag{8}$$

$$n = 1 + C_d / C_{ox} \tag{9}$$

are the depletion capacitance and subthreshold slope, respectively. The bulk-referenced gate-bias-dependent subthreshold surface potential is given by

$$\phi_{sub} = \left[-\frac{\gamma}{2} + \sqrt{\frac{\gamma^2}{4} + V_{gb} - V_{FB}} \right]^2 \tag{10}$$

Eqs. (3) and (7) are regarded as the piece-wise regional models, in which subthreshold is Ψ_s-based whereas strong inversion is V_t-based.

Since the bulk-referenced drain current (3) has the same form as the source-referenced model, our previously-developed analytical "drift + diffusion" model should still apply [4]:

$$I_{ds} = \beta_n V_{ge} = \beta_n \left(V_{gg} + V_{gd}\right), \tag{11}$$

that can be decomposed into the sum of the "drift" ($I_{drift} = \beta_n V_{gg}$) and "diffusion" ($I_{diff} = \beta_n V_{gd}$) currents, which approach the correct asymptotes in the strong-inversion and subthreshold regions, respectively. The key "smoothing" function is the "effective gate/drain voltage product" [5]:

$$V_{gg} = \frac{2 n v_{th} \ln\left(1 + e^{(V_{gs} - V_t)/(2 n v_{th})}\right) V_{de}}{1 + V_{de} \dfrac{2n\left(C_{ox}/C_d\right) e^{-(V_{gs} - V_t - 2V_{off})/(2 n v_{th})}}{v_{th}\left(1 - e^{-V_{ds}/v_{th}}\right)}} \tag{12}$$

which includes the effect of bulk charge

$$V_{de} = \left(1 - \frac{A_b}{2} \frac{V_{deff}}{V_{geff}}\right) V_{deff} . \tag{13}$$

V_{gd} is given by V_{gg}/W_{ge} to model the correct diffusion current in subthreshold without affecting drift current, where W_{ge} is derived to be [6]

$$W_{ge} = \frac{n}{A_b} \frac{e^{(V_{gs} - V_t)/(2 n v_{th})}}{1 - e^{-V_{ds}/v_{th}}} . \tag{14}$$

In the above equations, V_{geff} is the effective gate overdrive (BSIM interpolation function [2]), given by

$$V_{geff} = \frac{2 n v_{th} \ln\left(1 + e^{(V_{gs} - V_t)/(2 n v_{th})}\right)}{1 + 2n\left(C_{ox}/C_d\right) e^{-(V_{gs} - V_t - 2V_{off})/(2 n v_{th})}} \tag{15}$$

which approaches $V_{gs} - V_t$ in strong inversion. V_{deff} is the BSIM smoothing function [2]

$$V_{deff} = V_{dsat} - \tfrac{1}{2}\Big[V_{dsat} - V_{ds} - \delta_s + \sqrt{\left(V_{dsat} - V_{ds} - \delta_s\right)^2 + 4\delta_s V_{dsat}}\Big] \tag{16}$$

which approaches V_{ds} in linear region and

$$V_{dsat} = \frac{E_{sat} L_{eff} \left(V_{gs} - V_t\right)}{V_{gs} - V_t + A_b E_{sat} L_{eff}} \tag{17}$$

in saturation region, where $E_{sat} = 2v_{sat}/\mu_0$ is the saturation field, and δ_s is a fitting (smoothing) parameter.

To extract the model parameters, a 0.18-μm CMOS STI wafer is measured. Long-channel measured threshold voltages for different body biases have been extracted from the $I_{ds} - V_{gs}$ curves at low drain bias based on the constant-current definition. The effective channel doping and the flat-band voltage (N_{ch}, V_{FB}) are calibrated to the $V_t - V_{bs}$ data, and the semi-empirical mobility model [7] is then calibrated to the $I_{ds} - V_{gs}$ data at low drain and body biases. The smoothing parameter δ_s in (16), together with the channel-length modulation parameter (negligible for long channel), can be tuned to the $I_{ds} - V_{ds}$ data at high gate and low body biases [4].

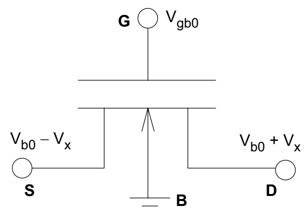

(a)

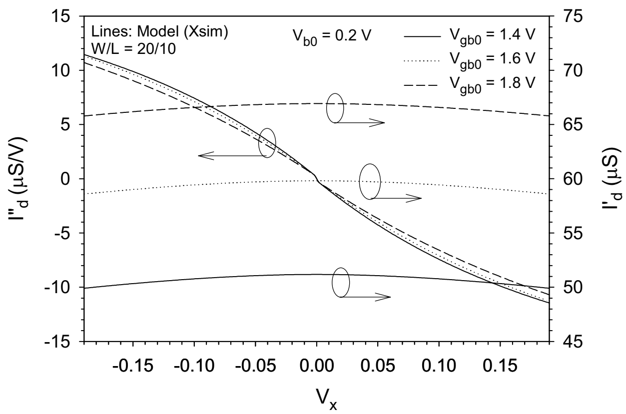

(b)

Figure 2: (a) The circuit diagram used for the Gummel symmetry test and (b) the first- and second-order derivatives of I_d with respect to V_x, exhibiting smooth transition at $V_x = 0$.

3 RESULTS AND DISCUSSION

The unified I_{ds} model has been calibrated to a 0.18-µm CMOS technology wafer, and the results are shown in Figs. 1–4 for the long-channel (10-µm) device (short-channel results are available but not shown in this paper). Figs. 1(a) and 1(b) show the fitted (and predicted for intermediate V_{bs}) $I_{ds} - V_{gs}$ characteristics in linear and saturation regions, respectively. Fig. 2 shows the circuit diagram [8] used for the Gummel symmetry test [9], and the first and second derivatives of drain current with respect to V_x. The smooth I_d'' at $V_x = 0$ confirms model symmetry. The negligible "glitch" in I_d'' at $V_x = 0$ may come from the non-unity slope of V_{deff} as V_{ds} approaches zero. Although this is an intrinsic problem in symmetry, it is negligible for practical values of δ_s. Fig. 3 shows the prediction of transconductance-to-current ratio versus V_{gs} for $V_{bs} = -0.9$ V and $V_{ds} = 0.1$ V. The figure shows no discontinuity or kink effect between the weak and strong-inversion regions, which demonstrates model smoothness. The inset of Fig. 3 shows the same data versus V_{gb} (left–botton axes) and versus I_{ds} (right–top axes), respectively. The V_{gb}-dependent g_m/I_{ds} in the subthreshold region is a result of the surface-potential-based modeling (ϕ_{sub}) in this region, which is consistent with the Gummel tree-top test [9].

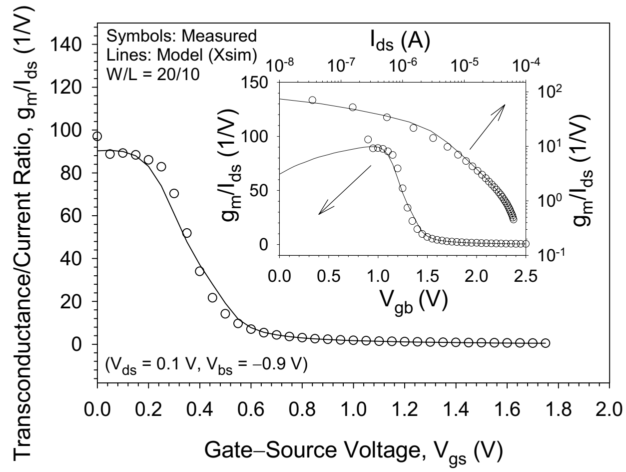

Figure 3: Predicted transconductance/current ratio at the terminal bias conditions indicated. The inset shows the same g_m/I_{ds} data versus V_{gb} (bottom–left) showing Gummel tree-top test; and versus I_{ds} (top–right) showing model smoothness.

Model prediction on higher-order derivatives of the drain current is shown in Fig. 4. Figs. 4(a) and 4(b) show the accurate prediction of the measured transconductance and output conductance versus gate and drain biases, respectively. Smooth transitions are observed between different regions [from weak to strong inversion in 4(a) and from linear to saturation region in 4(b)], even the second-order derivatives (g_m' and g_{ds}') are accurately predicted, as shown in the insets. The largest error occurs in g_m near $V_{gs} \approx V_t$, which is attributed to the interpolation function (V_{ge}) as well as inaccuracies in V_t. The intrinsic disadvantage of the regional model (as compared to the Ψ_s-based model) will be traded off with other advantages such as scalability and simplicity. Model continuity across regions of operation is an important criterion for analog circuit design, and our unified regional model has demonstrated model smoothness with reasonable accuracy as well as symmetry.

4 CONCLUSION

In conclusion, our previous source-referenced V_t-based (long-channel) drain current model is revised with bulk reference to preserve model symmetry, which uses only 9 parameters to characterize the entire range of operation and is capable of accurately predicting drain current and its higher-order derivatives with smooth transitions across different regions. Contrary to the general belief, our regional V_t-based model has demonstrated symmetry and continuity. This development maintains simple MOSFET equations that are familiar to circuit designers while removing major problems associated with the regional

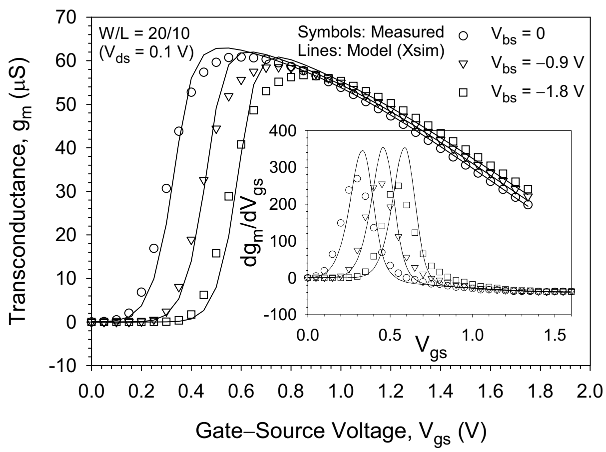

(a)

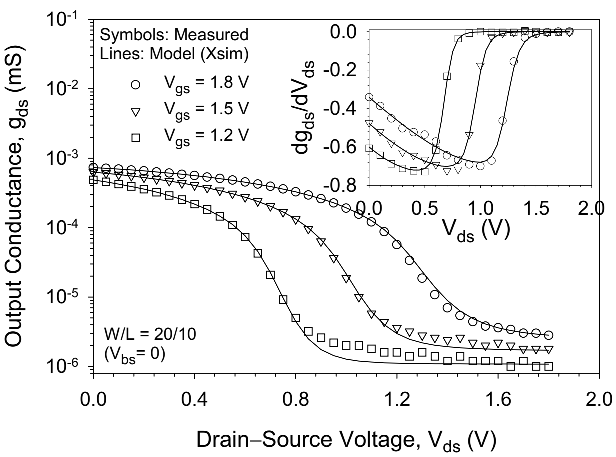

(b)

Figure 4: Prediction on the higher-order derivatives of drain current: (a) transconductance (and g_m' in the inset) and (b) output conductance (and g_{ds}' in the inset) at various terminal bias conditions indicated.

models. It serves as the starting point for the re-construction of our previously-developed unified scalable drain current model, Xsim [4]–[7], including short-channel effects, consistent charge-based intrinsic capacitances, and poly-depletion effect, to be presented elsewhere [10].

REFERENCES

[1] J. E. Meyer, "MOS models and circuit simulation," *RCA Rev.*, vol. 32, pp. 42–63, 1971.

[2] Y. Cheng, *et al.*, "BSIM3v3 Manual," Univ. of California, Berkeley, CA, 1997–1998.

[3] Y. Tsividis, "Operation and Modeling of the MOS Transistor," McGraw-Hill, 2nd ed., 1999.

[4] X. Zhou, S. B. Chiah, and K. Y. Lim, "A technology-based compact model for predictive deep-submicron MOSFET modeling and characterization," *Proc. Nanotech 2003*, Feb. 2003, vol. 2, pp. 266–269.

[5] X. Zhou and K. Y. Lim, "Unified MOSFET compact *I–V* model formulation through physics-based effective transformation," *IEEE Trans. Electron Devices*, vol. 48, no. 5, pp. 887–896, 2001.

[6] K. Y. Lim and X. Zhou, "MOSFET subthreshold compact modeling with effective gate overdrive," *IEEE Trans. Electron Devices*, vol. 49, no. 1, pp. 196–199, 2002.

[7] K. Y. Lim and X. Zhou, "A physically-based semi-empirical effective mobility model for MOSFET compact *I–V* modeling," *Solid-State Electron.*, vol. 45, no. 1, pp. 193–197,2001.

[8] K. Joardar, K. K. Gullapalli, C. C. McAndrew, M. E. Burnham, and A. Wild, "An improved MOSFET model for circuit simulation," *IEEE Trans. Electron Devices*, vol. 45, no. 1, pp. 134–148, 1998.

[9] "Benchmarks for compact MOSFET models," Electronic Industries Alliance, http://www.eig.org/eig/cmc

[10] X. Zhou, S. B. Chiah, K. Chandrasekaran, K. Y. Lim, L. Chan, and S. Chu, "Unified regional approach to consistent and symmetric DC/AC modeling of deep-submicron MOSFETs," *Proc. Nanotech 2004*, Mar. 2004.